ELSEVIER

Nuclear Instruments and Methods in Physics Research A 421 (1999) 342–351

NUCLEAR INSTRUMENTS & METHODS IN PHYSICS RESEARCH Section A

Six parameter patient registration directly from projection data

E.E. Fitchard[a,*], J.S. Aldridge[a], P.J. Reckwerdt[a], G.H. Olivera[a], T.R. Mackie[a], A. Iosevich[b]

[a] *Department of Medical Physics, University of Wisconsin-Madison, 1530 Medical Sciences Center, 1300 University Avenue, Madison, WI 53706-1532, USA*

[b] *Wright State University, Dayton, OH, USA*

Received 25 March 1998; received in revised form 17 July 1998

Abstract

Patient registration, a technique to ensure dose conformity, is an essential part of tomographic radiotherapy. A new six parameter (three translational and three angular) algorithm to implement this technique has been developed. The method is stable, accurate, and most importantly uses sinogram data as input, obviating image reconstruction. A sinogram, an array of Radon transforms, is derived directly from the raw data, which are photon transmission fluences from either a diagnostic or a megavoltage X-ray source. The algorithm uses properties of the Radon and Fourier transforms, such as the central slice theorem and Fourier shift theorem, to decouple translational and angular offsets. The theoretical underpinnings of this algorithm are presented here, whereas numerical verification using synthetic and experimental data is presented elsewhere.

PACS: 87.53.Tf; 87.53.-J; 87.56.-v

Keywords: Registration; Sinogram; Tomotherapy

1. Introduction

Cancer therapy embodies a variety of techniques to treat diseased regions of the body, for example, surgery, chemotherapy, and radiotherapy. In this paper we discuss the theoretical underpinnings of a relatively new radiation delivery technique referred to as *tomotherapy*. This method, as in traditional radiotherapy, delivers a tumoricidal dose of radiation to the diseased area over a series of daily treatments called fractions. However, in the case of tomotherapy, the intensity of the treatment beam is dynamically modulated while it traverses a helical path about the patient. This type of treatment, on the one hand, permits highly conformal delivery patterns, but on the other hand, it demands high spatial precision (errors on the order of $\pm$ 2 mm as opposed to $\pm$ 5 mm standard radiotherapy). The greater precision is important in sparing sensitive and normal tissues. A problem with any fractionated delivery system is verifying the patient position and correcting for offsets prior to each treatment. The offsets may be linear translations

* Corresponding author. Tel.: + 1 608 263 9529; e-mail: fitchard@madrad.radiology.wisc.edu.

0168-9002/99/$ – see front matter
PII: S0168-9002(98)01236-4

along all three coordinate axes and/or rotations about these three axes called, in aeronautical terminology, pitch, yaw, and roll. This angular terminology is used in lieu of the more standard Euler angles for two reasons: (1) the mechanical arrangement of the treatment table is such that only rotations about the coordinate axes are possible, and (2) the oncologists are accustomed to thinking in terms of pitch, yaw, and roll. In terms of Euler angles, (α, β, γ) as defined by Rose [1], we have the relations

$$\theta_{\text{pitch}} \rightarrow (-\pi/2, \theta_{\text{pitch}}, 0),$$

$$\theta_{\text{yaw}} \rightarrow (0, \theta_{\text{yaw}}, 0),$$

$$\theta_{\text{roll}} \rightarrow (\theta_{\text{roll}}, 0, 0). \quad (1)$$

The importance of algorithm efficiency is close to that of delivery precision, because the algorithm is used while the patient is lying on the couch awaiting treatment. For patient comfort and delivery reliability, it is desirable to minimize this time. To this end, the algorithm takes as input an initial or "gold standard" sinogram and one obtained just prior to treatment. This avoids the time consuming operation of image reconstruction. This paper concentrates on the theoretical basis of the algorithm; numerical verification can be found in other publications [2–4].

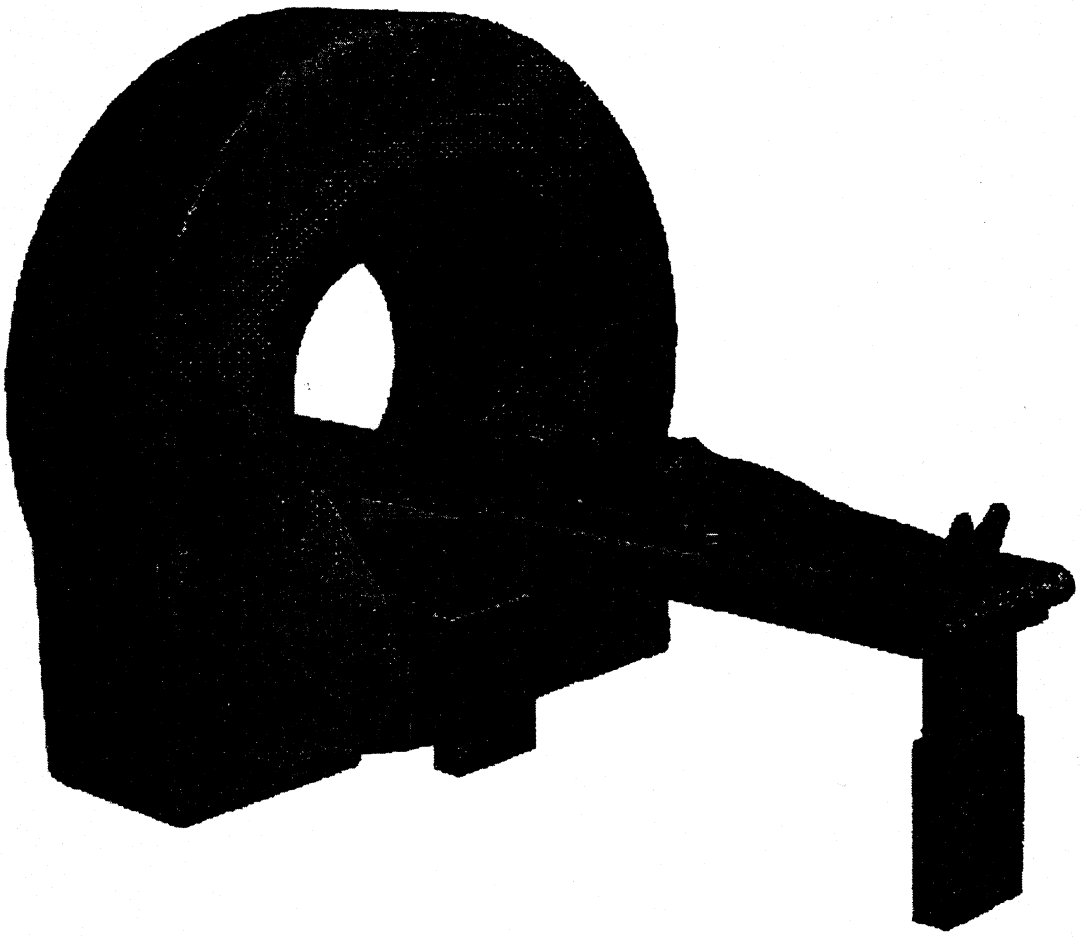

Fig. 1. Tomotherapy treatment machine. The patient is positioned on the table's conveyor belt prior to treatment. The source is rotated while the patient is moved through the treatment plane. A diagram of the megavoltage and diagnostic beams is shown in Fig. 2.

2. Computed tomography

The concept of tomotherapy is discussed in Mackie et al. [5,6]. Fig. 1 is an artist's conception of a tomotherapy machine. The main difference between this and a diagnostic CT unit is the presence of a megavoltage as well as a diagnostic fan-beam. The fan-beam labeled with a subscript k (see Fig. 2) consists of X-rays in the kilovoltage (diagnostic) energy range. The other fan-beam consists of X-rays in the megavoltage (therapy) energy range. The therapy treatment beam will be discussed later. Both of the sources are mounted on a CT-like rotating annular ring gantry from which radiation can be delivered while the patient is translated horizontally along the longitudinal axis. The path of the radiation source in a coordinate system "fixed" to the patient is helical. The fan-beams are intercepted by a curved detector, which measures the photon intensity, I, of a small subarc of the fan-beam. Each subarc is called a ray and is treated mathematically as a line. For modern machines the rays fan out from the "point" source. However, with older machines parallel rays were used. In these machines, the data were collected one ray at a time as the source moved perpendicular to the ray direction. Parallel rays are easier to handle mathematically and, to a good approximation, fan-beam rays can sometimes be approximated by parallel rays.

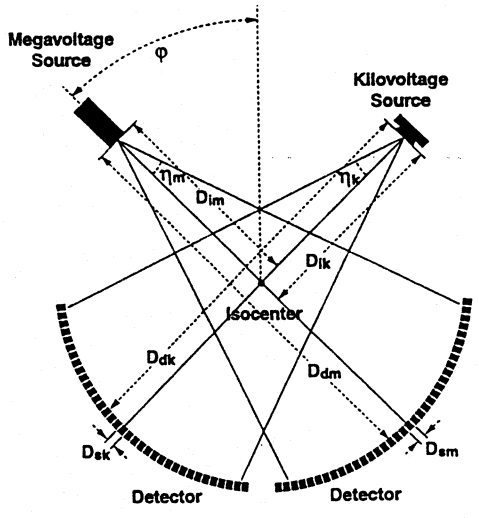

Fig. 2. Diagram of the sources and fan-beams with corresponding labels. The two fan-beams have central rays that are orthogonal and cross at the isocenter of the gantry. The gantry angle, φ, and fan-angle, η, are indicated. All of the quantities are subscripted with either an m (for megavoltage) or a k (for kilovoltage).

The intensity measured by the detectors is related to a property of the patient called the linear attenuation function, μ. This is a nonnegative, differentiable function in $\mathbb{R}^3$ of compact support. It is related to the density of the patient's tissues – greater for bone than for soft tissue and essentially zero for air. If the patient is moved a small distance, Δr, from his or her current position, the new attenuation function denoted as μ' has values satisfying the equation

$$\mu'(r) = \mu(r + \Delta r) + n(r). \tag{2}$$

The function $n(r)$ represents the noise in the data. Since this is random in nature, the functions μ and μ' will differ even if the offset $\Delta r = 0$. In the development of the algorithm, this term is ignored. Its effects will be manifested in the discrepancy between the experimental and computed results. The offset, Δr, can be determined from the maxima in the "cross-correlation" of the two attenuation functions. The cross-correlation of two real-valued functions in n-dimensions is defined by

$$(f \otimes_n g)(x) := \int_{\mathbb{R}^n} f(x + y)g(y)\,dy, \quad x,y \in \mathbb{R}^n. \tag{3}$$

If g is the same function (ignoring noise) as f translated by x_0 so that $g(y) = f(x_0 + y)$, then $(f \otimes_n g)(x)$ is maximum for $x = x_0$. This follows from the definition of the L^2 norm of a function and the Schwartz inequality. For an arbitrary function, μ, this may not be the only maximum. However, in tomotherapy the offset, x_0, is assumed to be small relative to the distance from the nearest local maximum. To demonstrate this, we have performed experiments with CT images from the "Visible Human Project" found on the web at "http://www.nlm.nih.gov/research/visible". These were processed to reduce the image size from 512 by 512 bytes to 256 by 256 bytes and to reduce the number of slices by half. Taking images from various parts of the body, cross-correlation functions have been

computed for a range of offsets. As expected, the global maximum at $x = 0$ is well separated from local extrema. Minimum distances are on the order of several centimeters, which is greater than the assumed initial offset of less than 1 cm. Fig. 3 is a plot the cross-correlation function for the upper legs of a human. The lower left-hand corner shows the image used. This example was chosen because it exhibits large side peaks. It is clear that none of the local extrema are near the global maximum. To emphasize this point, Fig. 4 zooms into a 10×10 cm^2 region centered at the global maximum. This and similar plots (not shown) verify that as long as the patient is initially near (within 1 or 2 cm) the global maximum, the registration method discussed will give a unique result. Typically, the initial patient position is within 1 cm of the global maximum. Tests images with 10% and 50% Gaussian random noise were also correlated. These demonstrated that noise has an insignificant influence.

The ratio of the photon intensity at a detector with the patient removed, I_0, to the intensity with

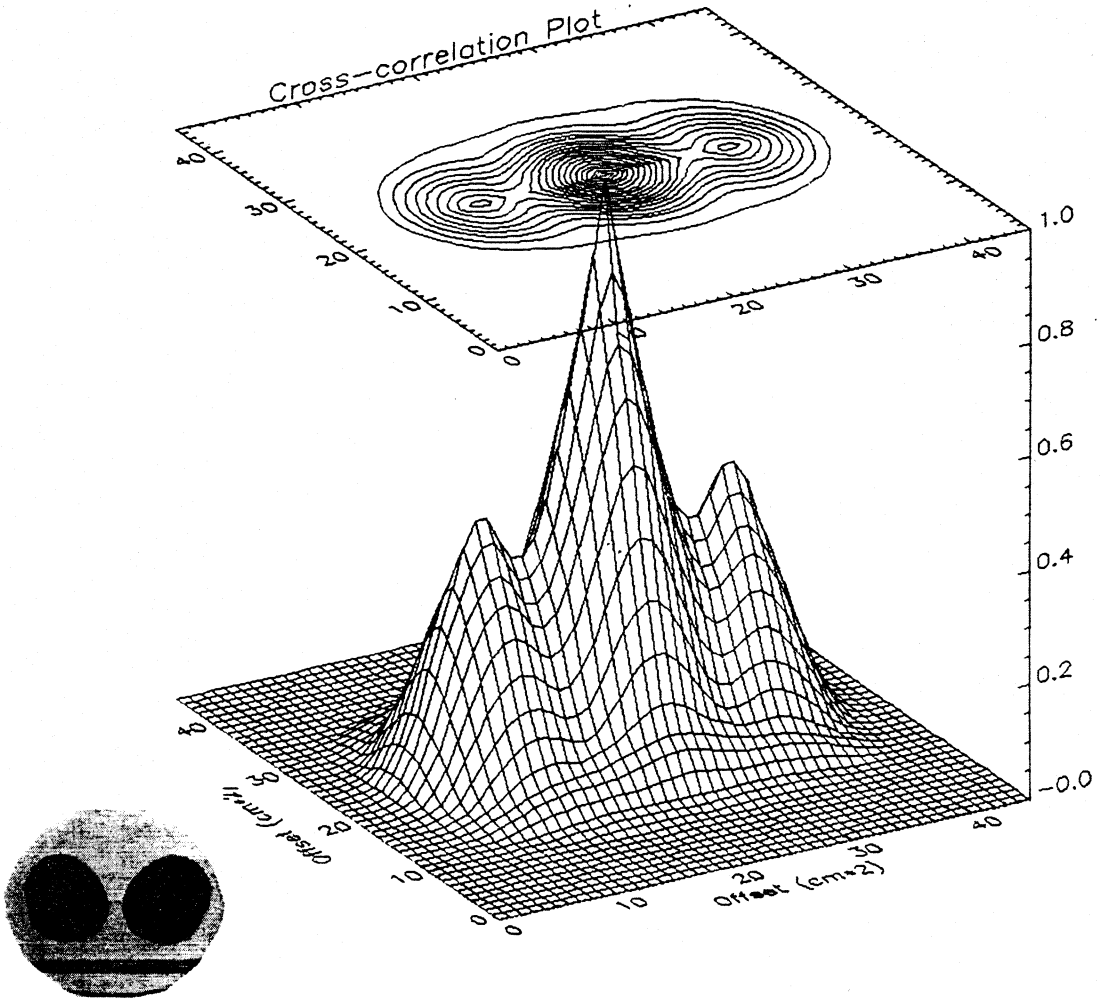

Fig. 3. Cross-correlation of 46×46 cm^2 image (lower left) of the upper legs of a human. The two prominent side peaks occur when the left leg overlaps the right or vice versa. The top contour plot demonstrates that the cross-correlation function has no peaks or valleys near the global maximum.

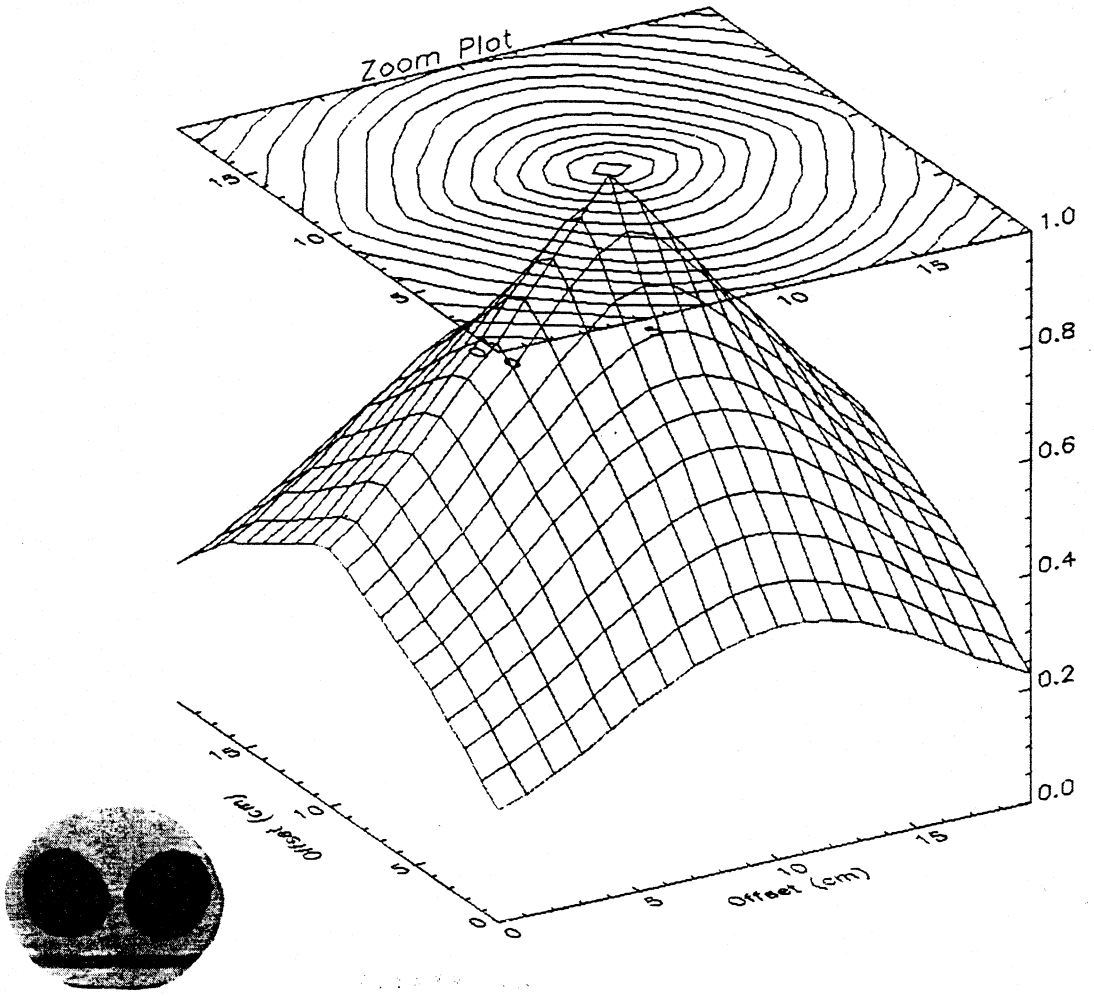

Fig. 4. A zoom of the previous figure into a region $20 \times 20\ \text{cm}^2$ about the global maximum. This emphasizes the conclusion that no local extrema occur within several cm of the global maximum.

the patient in place, I, is given by

$$\ln(I_0/I)(L) = \int_L \mu \, ds, \tag{4}$$

where L is the ray path of the photons, and ds is the one-dimensional Lebesgue measure on L. In the general case, we have to regard L as a line in $\mathbb{R}^3$. However, for "axial slices" we can regard L as a line in the plane. An axial slice is obtained by keeping the patient stationary while the gantry is rotated. For some purposes axial slices can be used in place of helical slices and are easier to work with mathematically. In this case the right-hand side of Eq. (4) reduces to a special case of the "Radon transform."

The Radon transform, as defined in Ref. [7], (Appendix A), of a function f on $\mathbb{R}^n$ is the function $Rf = \hat{f}$ on the set of hyperplanes of $\mathbb{R}^n$ given by

$$(Rf)(H) = \hat{f}(H) := \int_H f \, ds, \tag{5}$$

where ds is the Lebesgue measure on H. Thus, when the ambient space has dimension two, the right-hand side of Eq. (4) is simply the Radon transform of the attenuation function, μ, for the path, L. For the Radon transform in $\mathbb{R}^n$, we can write H nonuniquely as $H = \{r \in \mathbb{R}^n \mid \alpha \cdot r = p\}$ with α a unit vector in $\mathbb{R}^n$ and $p \in \mathbb{R}^1$; $H \leftrightarrow (\alpha, p)$ gives us a way to assign coordinates to the set of H's. The Radon transform can then be written symbolically as

$$(Rf)(\alpha,p) := \int_{\mathbb{R}^n} f(r)\delta(p - \alpha \cdot r)\, dr. \tag{6}$$

For axial slices, where $n = 2$, the array of Radon transforms for each path in the fan-beam, at one gantry angle, is called a profile. The two-dimensional array of profiles from each gantry angle is a projection data set, or sinogram. In the above notation, if $L \leftrightarrow (\alpha, p)$, we have

$$\ln (I_0/I)(L) = (R\mu)(\alpha,p) := \hat{\mu}(\alpha,p), \quad \alpha \in \mathbb{R}^2,$$
$$|\alpha| = 1, \quad p \in \mathbb{R}. \tag{7}$$

3. Tomotherapy

Just as in helical CT, helical tomotherapy radiation is delivered with the gantry and couch in simultaneous motion. While the patient travels through the gantry in the longitudinal direction, the rotating megavoltage fan-beam is modulated by a multileaf collimator (MLC) system. Helical tomotherapy also has the capability to blur the delivery between "slices," effectively eliminating junction artifacts (hot or cold spots in the high-dose region). In fact, the delivered dose is simply a single continuous band of intensity modulated radiation "custom made" to conform the dose to the target volume and possibly to "conformally avoid" any critical structures.

Dose conformity would be improved by allowing the X-rays to enter the patient from a full 4π geometry, however, this is precluded by engineering and practical problems. The human body has much greater length along the longitudinal direction than in the axial plane. Therefore, a machine that could send X-rays along the longitudinal axis would necessarily be much larger than current designs. Also, for tumors in the abdominal or thorax region, longitudinal X-rays traverse a considerable amount of normal and sensitive tissue. However, a larger interance solid angle can be obtained by dynamically tilting the gantry during the treatment. Except, perhaps in the case of head treatment, this does not significantly increase dose conformity, and it presents additional engineering and treatment planning problems, so it has not been attempted in the initial design.

The efficacy of tomotherapy has been tested experimentally using a computer-controlled phantom positioner and a megavoltage X-ray slit beam. These experiments [8,9] verify that helical beam treatments can deliver a uniform dose distribution to the target volume, provided the patient is correctly positioned.

3.1. Tomographic registration

Registration is a term that refers to the alignment of one patient image with another in such a way that they correspond point by point. Clearly, this is essential for any kind of radiation therapy, particularly when intensity modulated conformal and conformal avoidance treatments are being delivered. A variety of patient registration methods exist. External patient marks and laser alignment lights are currently used to obtain an overall patient setup in conventional radiotherapy. However, often skin alignment does not correspond to registration of a deep lying tumor, and more accurate techniques are warranted. To mitigate problems, a radiographic setup verification algorithm based on projection data collected prior to treatment has been developed. In tomotherapy the positioning requirements are more stringent, so these methods are supplemented by tomographic registration, a computer implemented algorithm that reduces the $\pm$ 5 mm positioning error of standard registration to less than $\pm$ 2 mm. This accuracy is possible by comparing the current and previously obtained (where, by assumption, the patient is correctly positioned) projection sets using cross-correlation. Prior to the first treatment, a patient would have a CT scan to obtain a projection set. This scan, which is a measure of the attenuation function, is

used to plan the treatment and also as a reference scan to position the patient before subsequent daily sessions are delivered. Registration of the patient position is done by cross-correlating the projection file acquired before the first treatment commences with the projection file acquired prior to the current daily treatment.

The Radon transform of an n-dimensional cross-correlation (indicated by the symbol, $\otimes_n$) of two functions is the 1-dimensional cross-correlation, in the second argument, of the Radon transformed functions. It can be shown from Eqs. (3), (5) and (6) that

$$\widehat{f \otimes_n g}\ (\alpha,p) = \hat{f}(\alpha,p) \otimes_1 \hat{g}(\alpha,p). \tag{8}$$

The derivation is essentially the same as that for the Radon transform of a convolution given in Deans ([7], pp. 72, 95), and Ramm and Katsevich ([10], pp. 15, 16). Note that the n-dimensional cross-correlation has been reduced to a set of one-dimensional cross-correlations labeled by the parameter α.

We shall make use of the Fourier transform, $\mathscr{F}$, which is defined by

$$(\mathscr{F}\mu)(k) := M(k) = \int_{\mathbb{R}^n} \mu(r) e^{ik\cdot r}\, dr, \quad k,r \in \mathbb{R}^n. \tag{9}$$

$$(\mathscr{F}^{-1}M)(r) = \frac{1}{(2\pi)^n} \int_{\mathbb{R}^n} M(k) e^{-ik\cdot r}\, dr. \tag{10}$$

The Fourier transform and Radon transform are related by the central slice theorem, which, stated symbolically, is

$$\mathscr{F}_{p\to t} R = \mathscr{F}, \tag{11}$$

where $\mathscr{F}_{p\to t}$ and $\mathscr{F}$ are a one-dimensional Fourier transform and the central slice of an n-dimensional Fourier transform, respectively. The proof (10, p. 15; 7, p. 128) is as follows:

$$\mathscr{F}f(t\alpha) = \int_{\mathbb{R}^n} f(x) e^{it\alpha\cdot x}\, dx = \int_{-\infty}^{\infty} e^{ipt} \times \int_{\mathbb{R}^n} f(x)\delta(p - \alpha\cdot x)\, dx\, dp = \mathscr{F}_{p\to t} Rf(\alpha,t), \tag{12}$$

where f satisfies the Dirichlet conditions.

4. Mathematical solution

4.1. Translational algorithm

The solution of the registration problem is based on the intuitive idea that the patient is correctly registered when the two-dimensional cross-correlation of the first and subsequent treatment attenuation functions are maximal. As pointed out in Section 2, this assumption is reasonable for medical tomotherapy. We start with this idea and show later how one can work directly with the projection sets. The arguments pertaining to Eq. (3) imply that the maximum condition for the cross-correlation can be expressed as

$$\frac{\partial}{\partial s_k} (\mu \otimes_2 \mu')(s)\Big|_{s=\Delta r} = 0, \quad k = 1,2, \quad s, \Delta r \in \mathbb{R}^2. \tag{13}$$

Here, μ' may include a translation and/or rotation about some point relative to the simulation position. However, for now only translations will be considered. The quantity s_k is the kth component of the cross-correlation variable, and Δr is the translation of the patient relative to the simulation position. The subscript k labels the x and y directions, respectively, in any convenient coordinate system. Typically, x is taken to lie in the horizontal direction and y in the vertical direction. The objective is to ascertain the direction and magnitude of the offsets.

One of the advantages of using a cross-correlation algorithm is that changes within the patient (i.e., small organ motion or tumor volume changes) will not defeat the algorithm. The cross-correlation array will change somewhat, however, the projection arrays are dominated by the patient surface (tissue to air density change) and bony structures (tissue and bone have a relatively large density difference). By comparison the movement of soft tissue organs will make only minor changes in the projection arrays. The maximum of the correlation array may be somewhat smaller, but it will occur at nearly the same values. This property (i.e., nonsensitivity to systematic or random error) is often referred to as algorithm stability. In numerical calculations with noisy data, a stable algorithm is essential.

If μ and μ' are known, Eq. (13) can be used directly. However, to compute these functions requires inversion of the Radon transform, which is a time consuming computation. It is preferable to work with projection files that are derived directly from measured data. From the definition of μ' in Eq. (2), it follows that

$$\hat{\mu}'(\alpha,p) = \int_{\mathbb{R}^3} \mu(r + \Delta r)\delta(p - \alpha\cdot r)\,\mathrm{d}r \tag{14}$$

$$= \int_{\mathbb{R}^3} \mu(r)\delta(p + \alpha\cdot\Delta r - \alpha\cdot r)\,\mathrm{d}r \tag{15}$$

$$= \hat{\mu}(\alpha,p + \Delta p), \tag{16}$$

where $\Delta p = \alpha\cdot\Delta r$. Thus, applying Eqs. (2), (3) and (16), the cross-correlation in projection space now becomes

$$(\hat{\mu}\otimes_1\hat{\mu}')(\alpha,p) = \int_{\mathbb{R}} \hat{\mu}(p + q)\hat{\mu}(q + \Delta p)\,\mathrm{d}q \tag{17}$$

$$\leq \|\hat{\mu}\|_{L^2(\mathbb{R})}. \tag{18}$$

By the same arguments as those leading to Eq. (8), we conclude that

$$\frac{\partial}{\partial q}(\hat{\mu}\otimes_1\hat{\mu}')(\alpha,q)\bigg|_{q=\Delta p} = 0. \tag{19}$$

Here, the symbol $\otimes_1$ stands for the one-dimensional cross-correlation in the second argument, which significantly decreases computation time compared to two- or three-dimensional cross-correlation. Note that evaluating s at Δr is equivalent to evaluating f at $p = \alpha\cdot\Delta r$. Eq. (19) is used to compute the patient linear offset from the measured data.

So far, we have assumed that μ' is not rotated relative to μ, as is indicated in Eq. (2). Suppose that μ'' is rotated, relative to μ', by an angle $\Delta\varphi$ about the rotation axis such that

$$\mu''(r) = \mu'(\mathscr{A}_{\Delta\varphi}^{-1}r), \tag{20}$$

where $\mathscr{A}_{\Delta\varphi}$ is the 2-by-2 rotation matrix for a counterclockwise rotation of $\Delta\varphi$. We write $(\mathscr{A}_{\Delta\varphi}\mu')(r)$ for the right side of Eq. (20). The Radon transform has the property ([7], p. 69)

$$R(\mathscr{A}_{\Delta\varphi}\mu')(\alpha,p) = \hat{\mu}'(\mathscr{A}_{\Delta\varphi}^{-1}\alpha,p). \tag{21}$$

This follows from the definition of the Radon transform and from the fact that the determinant of a rotation matrix is one. If we write $\alpha' = \mathscr{A}_{\Delta\varphi}^{-1}\alpha$, then $\hat{\mu}''(\alpha,p) = \hat{\mu}'(\alpha',p) = \hat{\mu}(\alpha', p + \Delta p)$, where $\Delta p = \alpha'\cdot\Delta r$ is the rotation invariant projection of the linear offset onto the profile. Now Eq. (19) takes the form

$$\frac{\partial}{\partial q}(\hat{\mu}\otimes_1\hat{\mu}'')(\alpha,q)\bigg|_{q=\Delta p} = 0. \tag{22}$$

This expression is used to obtain the offset magnitude and the offset direction relative to α'. The arguments leading to Eq. (22) depend on the assumption that the only maxima in the search region used for cross-correlation is the global maxima. With this assumption, verified by independent studies of human CT data, the same information is contained in Eqs. (13) and (22), however, registration using Eq. (22) avoids the time consuming computation of image reconstruction, and the accuracy can be greater if many projections are used.

4.2. Rotational algorithm

How then can the relative rotation be computed? To answer this question, we look at the magnitude of the Fourier transforms of the two attenuation functions. First, note that if the patient is rotated about some unknown position r_0 by an angle θ and then translated by a vector distance Δr the attenuation function $\mu'(r)$ is given by

$$\mu'(r) = \mu'(r - r_0 + r_0) = \mu[\mathscr{A}_\theta^{-1}(r - r_0) + r_0 + \Delta r]. \tag{23}$$

Although a different result would be obtained if the patient were first translated, in either case the transformation can be thought of as a rotation of the patient about the rotation axis followed by the appropriate translations. This can be illustrated by rewriting Eq. (23) as

$$\mu'(r) = \mu(\underbrace{\mathscr{A}_\theta^{-1}r}_{\text{Rotate}} - \underbrace{\mathscr{A}_\theta^{-1}r_0 + r_0 + \Delta r}_{\text{Translate}}) \tag{24}$$

or

$$\mu'(r) = \mu[\underbrace{\mathcal{A}_\theta^{-1}(-r_0 + \Delta r) + r_0}_{\text{Translate}} + \underbrace{\mathcal{A}_\theta^{-1} r}_{\text{Rotate}}] \tag{25}$$

Thus, in either case, the relative position of the patient consists of both a rotation about the isocenter and a translation, where the details of the translation terms depend on the actual center of rotation and the magnitude and direction of the translation. To determine the rotation, consider the two-dimensional Fourier transform of the attenuation function, Eq. (9) with $n = 2$:

$$M(k) = (\mathcal{F}\mu)(k), \quad k \in \mathbb{R}^2 \tag{26}$$

for the simulation position, and for the position prior to subsequent treatments,

$$M'(k) = (\mathcal{F}\mathcal{T}_{\Delta r_t}\mathcal{R})\mu(k), \tag{27}$$

where $\mathcal{T}_{\Delta r_t}$ is the translation operator, Δr_t is the unknown total translation in Eq. (24) or Eq. (25), and $\mathcal{R}$ is the rotation matrix for rotation about the z-axis with the angle of rotation suppressed. The Fourier shift property states that the Fourier transform of a translated function is a complex constant of unit magnitude times the Fourier transform of the untranslated function:

$$(\mathcal{F}\mathcal{T}_{\Delta r_t}\mathcal{R})\mu = e^{ik\cdot\Delta r_t}(\mathcal{F}\mathcal{R})\mu. \tag{28}$$

Thus, if we consider only the magnitude of the Fourier transforms, the offset and unoffset attenuation functions differ only by a relative rotation:

$$|(\mathcal{F}\mathcal{T}_{\Delta r_t}\mathcal{R})\mu| = |e^{ik\cdot\Delta r_t}(\mathcal{F}\mathcal{R})\mu|. \tag{29}$$

A simple calculation shows that the Fourier transform commutes with rotation. Therefore, Eq. (29) is

$$|e^{ik\cdot\Delta r_t}\mathcal{R}M(k)| = |\mathcal{R}M(k)|. \tag{30}$$

Since the magnitude of the Fourier transform depends only on the relative orientations of the simulation and pre-treatment attenuation functions, we can write an equation for rotation by analogy to Eq. (13):

$$\frac{\partial}{\partial\omega}(|M|\otimes_1|M'|)(|k|,w)\Big|_{\omega=\Delta\varphi} = 0. \tag{31}$$

Eq. (31) could be used to find the relative orientations of the two patient positions. However, as mentioned before, we wish to work only with projection data in order to avoid the computationally intensive operation of reconstruction. To get back into projection space, we use the central slice theorem and define this Radon transform as $\mathcal{F}_{p\to t}\hat{\mu}$. A proof similar to that preceding Eq. (8) can be constructed to show that

$$\frac{\partial}{\partial\omega}(|\mathcal{F}_{p\to t}\hat{\mu}|\otimes_1|\mathcal{F}_{p\to t}\hat{\mu}'|)(t,\omega)\Big|_{\omega=\Delta\varphi} = 0. \tag{32}$$

Using Eqs. (13) and (32) along with the measured tomographic data, one can compute the offset relative to the initial patient position. Once the relative offset of the patient is known, one can either physically move the patient back to the initial position or the treatment delivery can be adjusted by some method to correct for the relative offset.

5. Conclusion

In this article several basic ideas from mathematics and medical physics have been combined to produce a practical result with direct application to tomotherapy, a new cancer treatment methodology. The primary mathematical ideas are the Radon transform and its connection with the Fourier transform through the central slice theorem, as well as properties of the projection set space and its Fourier transform. Application of these mathematical concepts produces the translation and relative rotations directly from projection sets. The physical ideas are cross-correlation in real space, which is the intuitive method of overlaying images to determine the relative offsets, and the conversion of tomographic X-ray measurements to the Radon transform of rays through the patient. The connection between real space and projection space was demonstrated with the application of some transform properties. The amalgamation of mathematical and physical ideas has produced a practical

registration method which is both accurate (less than 1 mm error) and, efficient due to computation directly from projection data.

Acknowledgements

The authors, EEF, JSA, PJR, GHO and TRM would like to express their appreciation to GE Medical Systems for providing generous funding to the tomotherapy project. Their work was also supported by the NIH grant number CA48902. One author, AI, was partially supported by NSF Grant DMS 9706825.

References

[1] M.E. Rose, Elementary Theory of Angular Momentum, Wiley, New York, 1957.
[2] E.E. Fitchard, J.S. Aldridge, P.J. Reckwerdt, T.R. Mackie, Registration of Tomotherapy Patients Using CT Projection Files XII ICCR Salt Lake, Utah, USA 27–30 May, in: D.D. Leavitt, G. Starkschall (Eds.), Medical Physics Publishing, 1997, pp. 185.
[3] E.E. Fitchard, J.S. Aldridge, P.J. Reckwerdt, T.R. Mackie, Registration of synthetic tomotherapy projection data sets using cross-correlation, Phys. Med. Biol. 43 (1998) 1645.
[4] E.E. Fitchard, J.S. Aldridge, K. Ruchala, G. Fang, J. Balog, D.W. Pearson, G.H. Olivera, E.A. Schloesser, D. Wenman, T.R. Mackie, P.J. Reckwerdt, Registration using tomographic projection files, (1998) submitted.
[5] T.R. Mackie, T. Holmes, S. Swerdloff, P. Reckwerdt, J.O. Deasy, J. Yang, B. Paliwal, T. Kinsella, Tomotherapy: a new concept for the delivery of dynamic conformal radiotherapy, Med Phys. 20 (1993) 1709.
[6] T.R. Mackie, T.W. Holmes, P.J. Reckwerdt, J. Yang, Tomotherapy: optimized planning and delivery of radiation therapy, Int. J. Imaging Systems Tech. 6 (1995) 43.
[7] S.R. Deans, The Radon Transform and Some of its Applications, Wiley, New York, 1983.
[8] J.N. Yang, T.R. Mackie, P. Reckwerdt, J.O. Deasy, B.R. Thomadsen, An investigation of tomotherapy beam delivery, Med Phys. 3 (1997) 425.
[9] P.J. Reckwerdt, T.R. Mackie, J. Balog, T.R. McNutt, Three dimensional inverse treatment optimization for tomotherapy XII ICCR Salt Lake, Utah, USA 27–30 May, in: D.D. Leavitt, G. Starkschall(Eds.), Medical Physics Publishing, (1997), pp. 420.
[10] A.G. Ramm, A.I. Katsevich, The Radon Transform and Local Tomography, CRC Press, New York, 1996.